Journal of Solid State Chemistry 182 (2009) 246–252

Contents lists available at ScienceDirect

Journal of Solid State Chemistry

journal homepage: www.elsevier.com/locate/jssc

Enhanced quantum yield of yellow photoluminescence of Dy^{3+} ions in nonlinear optical $Ba_2TiSi_2O_8$ nanocrystals formed in glass

N. Maruyama, T. Honma, T. Komatsu *

Department of Materials Science and Technology, Nagaoka University of Technology, 1603-1 Kamitomioka-cho, Nagaoka 940-2188, Japan

ARTICLE INFO

Article history:
Received 4 September 2008
Received in revised form
23 October 2008
Accepted 26 October 2008
Available online 5 November 2008

PACS:
78.20.−e
78.20.Ci
81.05.Kf
81.05.Ys

Keywords:
Glass
Rare-earth ions
Photoluminescence
Quantum yield
Nanocrystal
Judd–Ofelt parameter

ABSTRACT

Transparent crystallized glasses consisting of nonlinear optical $Ba_2TiSi_2O_8$ nanocrystals (diameter: ~100 nm) are prepared through the crystallization of $40BaO–20TiO_2–40SiO_2–0.5Dy_2O_3$ glass (in the molar ratio), and photoluminescence quantum yields of Dy^{3+} ions in the visible region are evaluated directly by using a photoluminescence spectrometer with an integrating sphere. The incorporation of Dy^{3+} ions into $Ba_2TiSi_2O_8$ nanocrystals is confirmed from the X-ray diffraction analyses. The total quantum yields of the emissions at the bands of $^4F_{9/2}\rightarrow{}^6H_{15/2}$ (blue: 484 nm), $^4F_{9/2}\rightarrow{}^6H_{13/2}$ (yellow: 575 nm), and $^4F_{9/2}\rightarrow{}^6H_{11/2}$ (red: 669 nm) in the crystallized glasses are ~15%, being about four times larger compared with the precursor glass. It is found that the intensity of yellow (575 nm) emissions and the branching ratio of the yellow (575 nm)/blue (484 nm) intensity ratio increase largely due to the crystallization. It is suggested from Judd–Ofelt analyses that the site symmetry of Dy^{3+} ions in the crystallized glasses is largely distorted, giving a large increase in the yellow emissions. It is proposed that Dy^{3+} ions substitute Ba^{2+} sites in $Ba_2TiSi_2O_8$ nanocrystals.

1. Introduction

Photoluminescence (PL) of rare-earth (RE) ions in glassy or crystalline solids is one of the fundamental light-matter interactions and has been utilized for various photonic devices such as Nd^{3+}-doped solid state lasers and Er^{3+}-doped optical fiber amplifiers. Dy^{3+} ions in solids show yellow (~570 nm) emissions resulting from the *f–f* transition of $^4F_{9/2}\rightarrow{}^6H_{13/2}$ and 1.3 μm emissions due to the $^6F_{11/2}$, $^6H_{9/2}\rightarrow{}^6H_{15/2}$ transition, and these emissions have been considered to be utilized as visible solid state lasers and optical amplifiers in broad band telecommunication systems. Since PL properties of RE ions depend on the structural and chemical bonding states of RE ions in a given host material, it is of interest and importance to search materials giving intense yellow or 1.3 μm emissions for photonic device applications of Dy^{3+} ions. Many studies on PL properties of Dy^{3+} ions in glasses have been reported so far [1–5]. For instance, Tanabe et al. [1] reported that the relative intensity of yellow emissions of Dy^{3+} ions in $xNa_2O–(95-x)B_2O_3–5CaO$ glasses increases with increasing Na_2O content. Further studies on quantitative analyses for yellow emissions of Dy^{3+} ions in glasses are strongly required.

On the other hand, nanostructures are the gateway into a new realm in physical, chemical, biological, and materials science. Crystallization of glass is one of the effective methods for fabrication of nanostructures [6], and recently new optically transparent bulk nanocrystallized glasses (glass-ceramics) have been successfully fabricated in some glasses [7–10]. Among them, transparent nanocrystallized glasses consisting of nonlinear optical/ferroelectric nanocrystals have received much attention, because such materials have a high potential for applications in photonic devices such as tunable waveguide and optical switching [11,12]. In RE-doped nonlinear optical/ferroelectric crystals, laser emissions in the short-wavelength region have been expected through self-frequency doubling (SFD) phenomena [13,14]. It is, therefore, of interest and importance to develop RE-doped transparent crystallized glasses with nonlinear optical nanocrystals and to clarify the features of RE ions in nanocrystals. It should be pointed out that the reports on incorporations and optical properties of RE ions in transparent crystallized glasses with nonlinear optical crystals are a few [15–17]. Recently, there have been numerous reports on incorporations and fluorescence properties of RE ions in fluoride nanocrystals such as LaF_3 or

* Corresponding author. Fax: +81 258 47 9300.
E-mail address: komatsu@mst.nagaokaut.ac.jp (T. Komatsu).

0022-4596/$ - see front matter © 2008 Elsevier Inc. All rights reserved.
doi:10.1016/j.jssc.2008.10.028

CaF_2 formed in transparent oxyfluoride crystallized glasses [18,19]. But, fluoride nanocrystals reported so far are centrosymmetric crystals inducing no second harmonic generations (SHGs).

Very recently, Maruyama et al. [17] synthesized transparent crystallized glasses consisting of nonlinear optical Nd^{3+}, Er^{3+}-doped $Ba_2TiSi_2O_8$ nanocrystals in $40BaO–20TiO_2–40SiO_2$ glasses and clarified the features of optical properties of Nd^{3+} and Er^{3+} ions. In particular, they proposed from the Judd–Ofelt analyses that the site symmetry of Nd^{3+} and Er^{3+} ions in nanocrystallized glasses is largely distorted due to their incorporations into Ba^{2+} sites in $Ba_2TiSi_2O_8$ nanocrystals. Since it is expected that PL intensities of RE ions being located at distorted sites are enhanced, it is of interest to clarify PL quantum efficiencies of RE ions quantitatively in $Ba_2TiSi_2O_8$ nanocrystals.

In this study, Dy^{3+}-doped $Ba_2TiSi_2O_8$ nanocrystals are synthesized through the crystallization of Dy_2O_3-doped $40BaO–20TiO_2–40SiO_2$ glasses and examined PL properties of Dy^{3+} ions in the visible region. In particular, the quantitative quantum efficiency for yellow (~570 nm) emissions is measured directly by using a PL spectrometer with an integrating sphere. It is found that the quantum efficiency for yellow emissions of Dy^{3+} ions is largely enhanced through the incorporation into $Ba_2TiSi_2O_8$ nanocrystals in comparison with Dy^{3+} ions present in the precursor glass. It is known that the intensity of the $^4F_{9/2}\rightarrow{}^6H_{13/2}$ transition of Dy^{3+} ions giving yellow emissions in glasses depends largely on the local symmetry of coordination environments around Dy^{3+} ions [1–5]. It is also pointed out that studies on the direct measurements of PL quantum efficiencies of RE ions in the visible region are scarce.

2. Experimental

A glass with the composition of $40BaO–20TiO_2–40SiO_2–0.5Dy_2O_3$ (in the molar ratio) was prepared using a conventional melt-quenching method. The composition of $40BaO–20TiO_2–40SiO_2$ corresponds to that of the $Ba_2TiSi_2O_8$ crystalline phase, and the glass is designated here as BTS glass. Commercial powders of reagent grade $BaCO_3$, TiO_2, SiO_2, and Dy_2O_3 were mixed and melted in a platinum crucible at 1500 °C for 1 h in an electric furnace. The batch weight was 20 g. The glass transition, T_g, and crystallization peak, T_p, temperatures were determined using differential thermal analyses (DTA) at a heating rate of 10 K/min. The glasses were mechanically polished to a mirror finish with diamond slurries and then were heat treated using a two-step heat treatment method to get transparent nanocrystallized glasses: first the glasses were heat treated at 745 °C for 1 h (nucleation) and then further heat treated at 760–800 °C for 30 min (crystal growth) [17].

The crystalline phase present in the heat-treated samples was examined by X-ray diffraction (XRD) analyses at room temperature using Cu$K\alpha$ radiation. Refractive indices at a wavelength of 632.8 nm (He–Ne laser) were measured with a prism coupler (Metricon Model 2010) at room temperature. Densities of the precursor glass and crystallized glasses were determined by means of Archimedes method using distilled water as an immersion liquid. Optical absorption spectra for the samples with a thickness of around 1 mm were taken in the wavelength range of 300–2000 nm on a Shimadzu UV-3150 spectrometer. All optical absorption spectra were corrected by subtracting the reflectance at the surface obtained from the Fresnel's equation. The PL quantum efficiencies in the visible region of Dy^{3+} ions were measured with a PL spectrometer with an integrating sphere (Hamamatsu Photonics: Absolute PL Quantum Yield Measurement System C9920-20) at room temperature, in which the excitation light with a wavelength of $\lambda = 352$ nm was used. SHGs of crystallized glasses were examined by measuring second harmonic (SH) waves ($\lambda = 532$ nm) for the incident light of a Q-switched Nd:YAG (yttrium aluminum garnet) laser with $\lambda = 1064$ nm. As a polarization on SH intensity measurements, the combination of p-excitation and p-detection (p–p polarization) was used.

3. Results and discussion

3.1. Transparent crystallized glasses with Dy^{3+}-doped $Ba_2TiSi_2O_8$ nanocrystals

The crystallization behavior of $BaO–TiO_2–SiO_2$ glasses has been examined in detailed by several authors so far, and a prominent nanocrystallization forming nonlinear optical $Ba_2TiSi_2O_8$ nanocrystals has been clarified, in particular, in $40BaO–20TiO_2–40SiO_2$ glass, i.e., BTS glass [17,20–22]. The XRD patterns at room temperature for the samples obtained by heat treatments at 760–800 °C for 30 min in Dy_2O_3-doped BTS glass are shown in Fig. 1. All XRD peaks are assigned to the so-called fresnoite $Ba_2TiSi_2O_8$ crystalline phase (space group P4bm, JCPDS: no.022-0513), indicating the formation of only $Ba_2TiSi_2O_8$ crystals. It was found that the position in the peaks assigned to $Ba_2TiSi_2O_8$ crystals shifts towards higher angles due to the addition of Dy_2O_3. The lattice constants of $Ba_2TiSi_2O_8$ crystals with a tetragonal structure in Dy_2O_3-doped crystallized (820 °C, 30 min) glass were estimated to be $a = 0.8543$ nm and $c = 0.5238$ nm. On the other hand, $Ba_2TiSi_2O_8$ crystals in the crystallized glasses containing no Dy_2O_3 showed the values of $a = 0.8543$ nm and $c = 0.5251$ nm. It is, therefore, noted that in particular, the c-axis length was shortened in Dy_2O_3-doped sample. The ionic radii of Ba^{2+} and Dy^{3+} ions in the eight oxygen coordinated state are 0.142 and

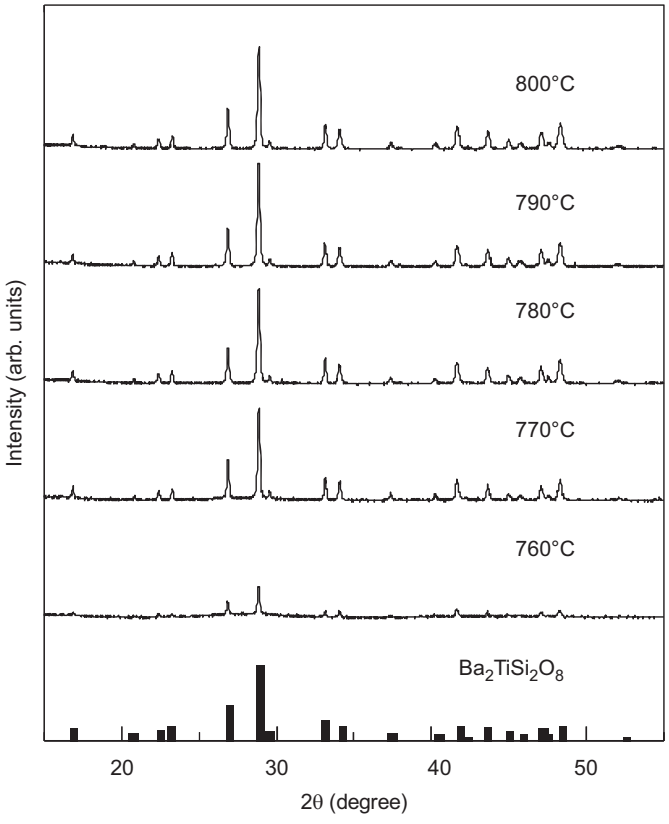

Fig. 1. XRD patterns at room temperature for the samples obtained by heat treatments at 760–800 °C for 30 min in $40BaO–20TiO_2–40SiO_2–0.5Dy_2O_3$ glass.

0.1027 nm, respectively [23]. The XRD results suggest the incorporation of Dy^{3+} into $Ba_2TiSi_2O_8$ crystals.

The values of the density and the refractive index for the crystallized glasses are listed in Table 1. It is found that the density increases with increasing heat treatment temperature, and contrarily, the refractive index decreases due to the formation of $Ba_2TiSi_2O_8$ nanocrystals. The volume fraction of $Ba_2TiSi_2O_8$ nanocrystals in the heat-treated samples, f, was estimated from the density of the heat-treated samples, d(sample), using the following equation:

$$d(sample) = (1-f)d(glass) + fd(Ba_2TiSi_2O_8) \quad (1)$$

where d(glass) is the density of the precursor BTS glass, i.e., 4.328 g/cm^3 and $d(Ba_2TiSi_2O_8)$ is the density of $Ba_2TiSi_2O_8$ crystals [24], i.e., 4.446 g/cm^3. From Eq. (1), the following volume fractions were obtained, i.e., $f = 0.10$, 0.64, and 0.71 for the samples heat-treated at 760, 780, and 800 °C for 30 min, respectively.

The optical absorption spectra at room temperature for the precursor BTS glass and crystallized (780 °C, 30 min) glass are shown in Fig. 2, in which the optical photographs for these samples are included. The typical transitions between the ground state of $^6H_{15/2}$ and the excited states of ^6F_J and $^6H_{11/2}$ in Dy^{3+} ions are observed in both samples, and the peak assignments are given in the figure. As can be seen in Fig. 2, the crystallized sample keeps a good optical transparency, but the absorption edge shifts towards a longer wavelength due to the crystallization. Similar optical absorption spectra were obtained in other crystallized (760~800 °C) glasses. Furthermore, it is seen that the position (~1280 nm) of the peak assigned to the $^6H_{15/2} \rightarrow {}^6F_{11/2}$ transition shifts to a longer wavelength. The average particle sizes of $Ba_2TiSi_2O_8$ crystals in Dy_2O_3-doped crystallized glasses were estimated from the peak width of XRD patterns (Fig. 1) by using the Scherrer's equation and were found to be 70–150 nm. The particle size of $Ba_2TiSi_2O_8$ crystals in the transparent crystallized glasses of $40BaO–20TiO_2–40SiO_2$ has been reported to be 100–200 nm [20–22]. The results shown in Figs. 1 and 2, therefore, suggest that transparent crystallized glasses consisting of $Ba_2TiSi_2O_8$ nanocrystals are fabricated in $40BaO–20TiO_2–40SiO_2–0.5Dy_2O_3$ glass.

We carried out SHG experiments for transparent crystallized glasses consisting of $Ba_2TiSi_2O_8$ nanocrystals and confirmed SHGs. As an example, the Maker fringe pattern for the transparent crystallized sample obtained by a heat treatment at 790 °C for 30 min is shown in Fig. 3. The data for the crystallized sample of $40BaO–20TiO_2–40SiO_2$ with no Dy_2O_3 are also shown in Fig. 3. The SHGs are clearly detected, and the Maker fringe pattern being typical for nonlinear optical crystals with no orientations is observed. It is noted that the SH intensities for the Dy^{3+}-doped sample are almost the same as those for the Dy^{3+} undoped sample. The SH intensities are shown in Fig. 4 as a function of heat treatment temperature, suggesting that SH intensities increase with increasing the volume fraction of $Ba_2TiSi_2O_8$ nanocrystals. The results shown in Figs. 3 and 4 demonstrate that $Ba_2TiSi_2O_8$ nanocrystals formed through the crystallization of $40BaO–20TiO_2–40SiO_2–0.5Dy_2O_3$ glass are nonlinear optical crystals. Takahashi et al. [21] reported similar results for the transparent crystallized glasses of $40BaO–20TiO_2–40SiO_2$ with no Dy_2O_3.

Table 1
Density d, refractive index n, and Judd–Ofelt parameters Ω_t ($t = 2, 4, 6$) of the glass and crystallized glasses of $40BaO–20TiO_2–40SiO_2–0.5Dy_2O_3$.

Sample	d (g/cm^3; ±0.003)	n (±0.0001)	Ω_t (10^{-20} cm^2)		
			Ω_2	Ω_4	Ω_6
Base glass	4.328	1.7787	4.97	0.60	0.68
Heat-treated					
760 °C, 30 min	4.340	1.7769	5.66	0.58	0.76
770 °C, 30 min	4.375	1.7723	8.61	0.92	0.81
780 °C, 30 min	4.404	1.7692	11.1	0.86	0.72
790 °C, 30 min	4.409	1.7665	11.8	1.36	1.00
800 °C, 30 min	4.412	1.7661	11.9	1.80	0.99

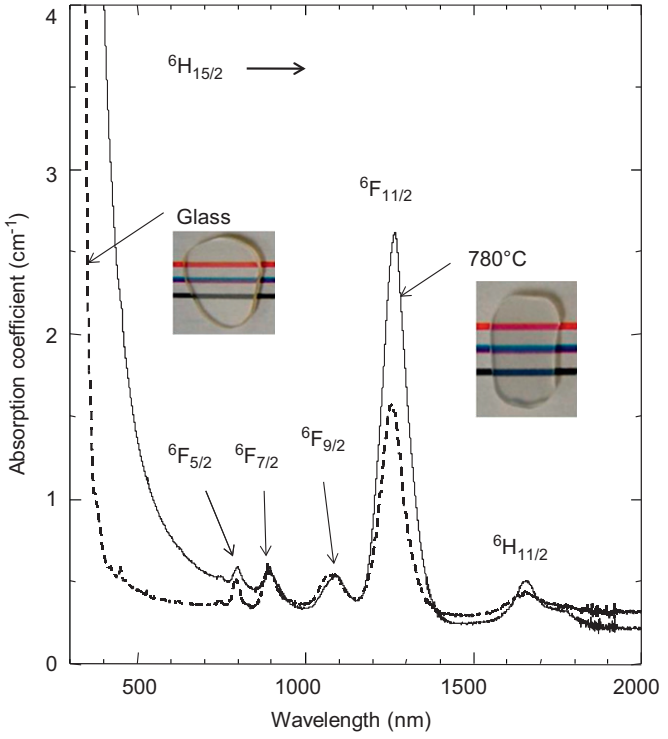

Fig. 2. Optical absorption spectra at room temperature for the precursor BTS and crystallized (780 °C, 30 min) glasses containing Dy^{3+} ions. The optical photographs for these samples are also shown.

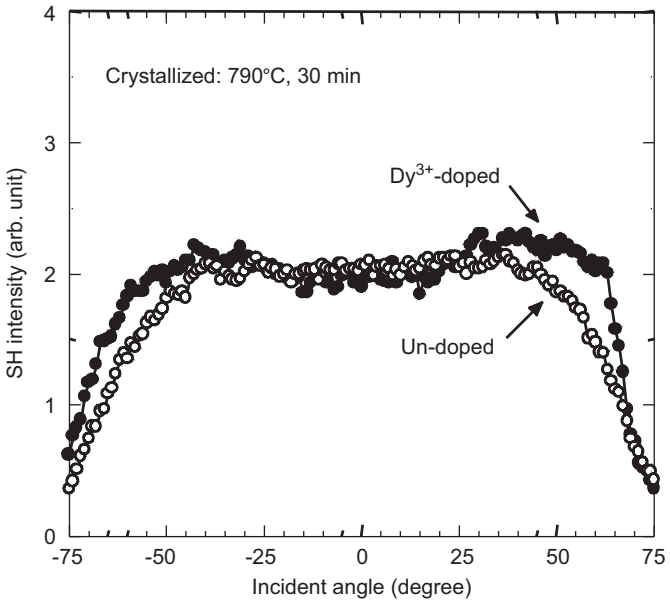

Fig. 3. Maker fringe pattern of SH intensities for the crystallized (790 °C, 30 min) sample of $40BaO–20TiO_2–40SiO_2–0.5Dy_2O_3$ glass. The data for the sample containing no Dy_2O_3 are also shown.

3.2. PL quantum efficiency of Dy^{3+} ions

The PL spectra in the range of 450–700 nm obtained in the experiments of quantum yield measurements for the precursor BTS and crystallized (at 770 and 790 °C, for 30 min) glasses of $40BaO–20TiO_2–40SiO_2–0.5Dy_2O_3$ are shown in Fig. 5. Three peaks assigned to the *f–f* transitions of $^4F_{9/2}\rightarrow{}^6H_{15/2}$ (blue: 484 nm), $^4F_{9/2}\rightarrow{}^6H_{13/2}$ (yellow: 575 nm), and $^4F_{9/2}\rightarrow{}^6H_{11/2}$ (red: 669 nm) are observed. It is seen that the intensity of these peaks increases due to the crystallization. In particular, the crystallized samples show the strong intensity for the peak corresponding to the $^4F_{9/2}\rightarrow{}^6H_{13/2}$ transition compared with the precursor BTS glass.

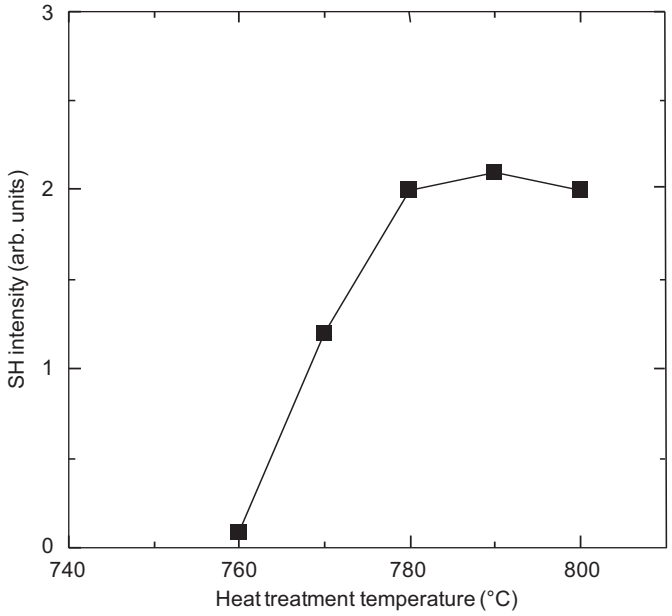

Fig. 4. Second harmonic intensities as a function of heat treatment temperature for the crystallized glasses of $40BaO–20TiO_2–40SiO_2–0.5Dy_2O_3$.

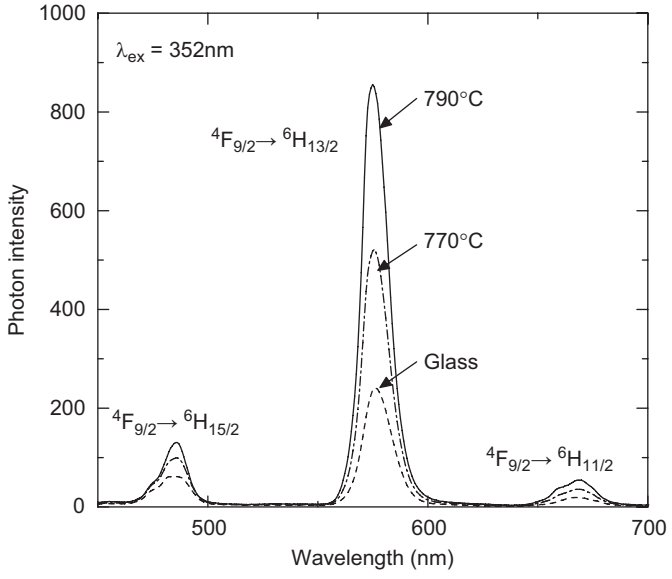

Fig. 5. Photoluminescence spectra of Dy^{3+} ions in the range of 450–700 nm obtained in the quantum yield measurements for the precursor BTS and crystallized (770 and 790 °C, 30 min) glasses. The wavelength of the excitation light was 352 nm.

The total quantum yields of the emissions at the bands of $^4F_{9/2}\rightarrow{}^6H_{15/2}$ (484 nm), $^4F_{9/2}\rightarrow{}^6H_{13/2}$ (575 nm), and $^4F_{9/2}\rightarrow{}^6H_{11/2}$ (669 nm) in the visible region for the precursor BTS glass and crystallized glasses at room temperature are shown in Fig. 6. The glass shows the quantum yield of 4.1%. It is seen that the quantum yield increases gradually due to the crystallization, and the crystallized glass obtained by a heat treatment at 790 °C for 30 min indicates the value of 15.2%, being close to four times in comparison with the value for the glass. The emission intensity ratio of $R = I(^4F_{9/2}\rightarrow{}^6H_{13/2})/I(^4F_{9/2}\rightarrow{}^6H_{15/2})$, i.e., the yellow/blue intensity ratio, was estimated from the spectra, and the results are shown in Fig. 7. It is found that the yellow/blue intensity ratio increases due to the crystallization. The crystallized (790, 800 °C) glasses show the values of nearly $R = 8$. That is, the contribution of the yellow emission is large in the crystallized glasses. The results shown in Figs. 5–7 suggest that the site environment of Dy^{3+} ions changes largely due to the crystallization.

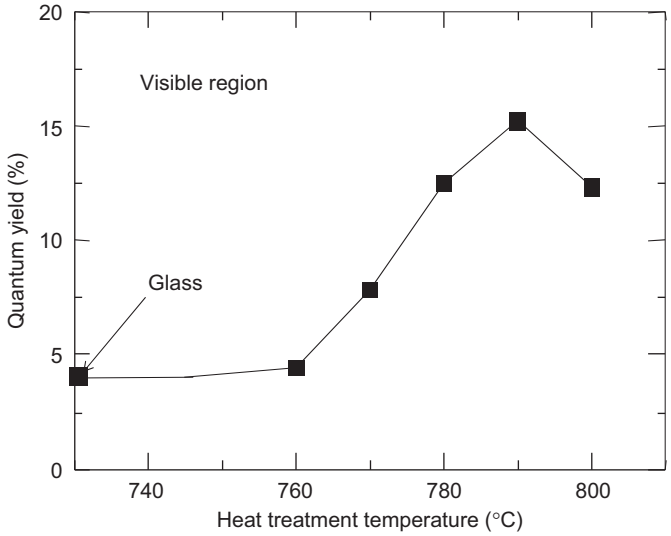

Fig. 6. Total quantum yields of the emissions at the bands of $^4F_{9/2}\rightarrow{}^6H_{15/2}$ (484 nm), $^4F_{9/2}\rightarrow{}^6H_{13/2}$ (575 nm), and $^4F_{9/2}\rightarrow{}^6H_{11/2}$ (669 nm) of Dy^{3+} ions in the visible region for the precursor BTS glass and crystallized glasses.

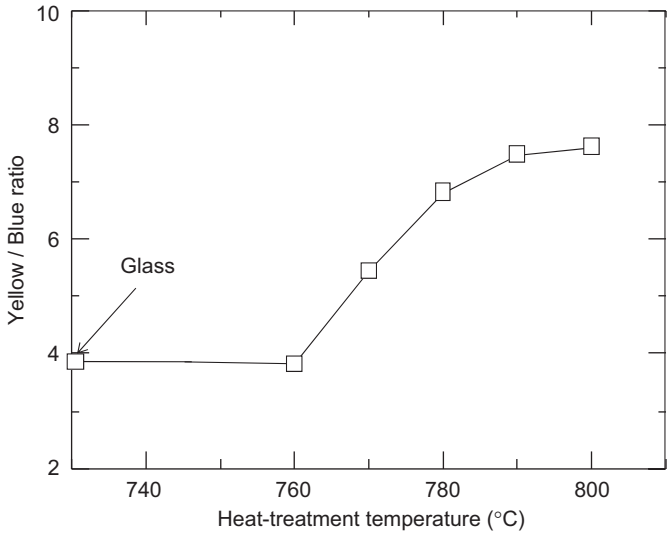

Fig. 7. Emission intensity ratio of $R = I(^4F_{9/2}\rightarrow{}^6H_{13/2})/I(^4F_{9/2}\rightarrow{}^6H_{15/2})$, i.e., the yellow/blue intensity ratio for Dy^{3+} ions in the precursor BTS glass and crystallized glasses.

3.3. Mechanism of enhanced quantum yields for yellow emissions

Numerous studies on the Judd–Ofelt Ω_t parameters ($t = 2$, 4, and 6) of RE ions in glasses have been carried out so far, and their origins have been discussed [25–28]. It has been well recognized that the Ω_t parameters, especially Ω_2 parameter, depend on the asymmetry and the covalency of RE ion sites in glasses. That is, the Ω_2 parameter increases with increasing site distortion of RE ions and with increasing the covalency of RE–O bonds. The parameters of Ω_4 and Ω_6 might be related to the rigidity of host glasses. Very recently, Maruyama et al. [17] evaluated the Judd–Ofelt parameters, Ω_t of Nd^{3+} and Er^{3+} ions in the crystallized glasses consisting of $Ba_2TiSi_2O_8$ nanocrystals in $40BaO–20TiO_2–40SiO_2–0.5Nd_2O_3$ or $0.5Er_2O_3$. They found that the Ω_2 parameter of Nd^{3+} and Er^{3+} increases largely due to the crystallization and proposed that the site symmetry of Nd^{3+} and Er^{3+} ions in crystallized glasses is largely distorted due to their incorporations into the Ba^{2+} sites in $Ba_2TiSi_2O_8$ nanocrystals. The change in the Ω_4 and Ω_6 parameters due to the crystallization is small [17].

The Judd–Ofelt Ω_t parameters of Dy^{3+} ions in the crystallized glasses of $40BaO–20TiO_2–40SiO_2–0.5Dy_2O_3$ prepared in this study were evaluated from the absorption spectra shown in Fig. 2. The procedures are given in the previous paper [17]. The results for the Ω_t parameters are shown in Fig. 8 and Table 1. The values of $\Omega_2 = 4.97$, $\Omega_4 = 0.60$, $\Omega_6 = 0.68 \times 10^{-20}\,cm^2$ were obtained for the precursor glass, and for instance, the crystallized (790 °C, 30 min) glass with $Ba_2TiSi_2O_8$ nanocrystals shows the values of $\Omega_2 = 11.8$, $\Omega_4 = 1.36$, and $\Omega_6 = 1.00 \times 10^{-20}\,cm^2$. In order to evaluate the validity of the Judd–Ofelt parameters Ω_t obtained by the fitting, the root mean square values, δ_{rms}, were calculated using the measured and calculated line strengths. The procedure is given in Ref. [29]. The average value of $\delta_{rms} = 8\%$ was obtained, and it would be possible to discuss the change in the Judd–Ofelt parameters, in particular, the Ω_2 parameter, due to nanocrystallization, because the change in the Ω_2 parameter is extremely large, i.e., over 200% increase as depicted in Table 1. It is seen that, in particular, the value of Ω_2 increases largely and monotonously due to the crystallization. On the other hand, the change in the Ω_4 and Ω_6 parameters due to the crystallization is small. These results are similar to the cases of Nd^{3+} and Er^{3+} [17].

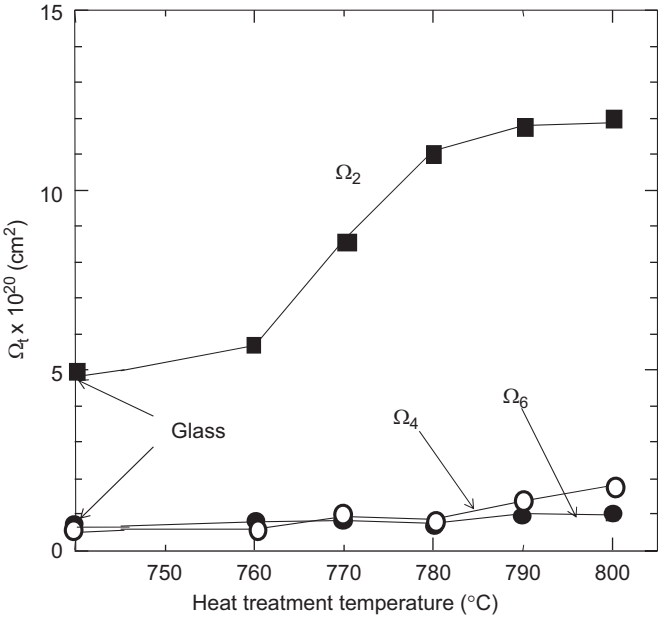

Fig. 8. Values of the Judd–Ofelt Ω_t parameter of Dy^{3+} ions as a function of heat treatment temperature in the precursor BTS and crystallized glasses.

Table 2
Reduced matrix elements of $U^{(t)}$ and expected wavelengths for the f–f transitions of Dy^{3+} ions (Ref. [1]).

f–f Transition state	$(U^{(2)})^2$	$(U^{(4)})^2$	$(U^{(6)})^2$	λ (nm)
$^4F_{9/2} \rightarrow {}^6H_{15/2}$	0.0	0.0046	0.0292	480
$^4F_{9/2} \rightarrow {}^6H_{13/2}$	0.0490	0.0164	0.0545	570
$^4F_{9/2} \rightarrow {}^6H_{11/2}$	0.0093	0.0018	0.0033	660

The reduced matrix elements of $U^{(t)}$ in the Judd–Ofelt theory for the f–f transition of $^4F_{9/2} \rightarrow {}^6H_{15/2}$ (484 nm), $^4F_{9/2} \rightarrow {}^6H_{13/2}$ (575 nm), and $^4F_{9/2} \rightarrow {}^6H_{11/2}$ (669 nm) for Dy^{3+} ions reported by Tanabe et al. [1] are given in Table 2. It should be pointed out that the f–f transitions are mainly dominated by $U^{(6)}$ for $^4F_{9/2} \rightarrow {}^6H_{15/2}$ (484 nm) and $U^{(2)}$ and $U^{(6)}$ for $^4F_{9/2} \rightarrow {}^6H_{13/2}$ (575 nm), respectively. The $U^{(t)}$ values for $^4F_{9/2} \rightarrow {}^6H_{11/2}$ (669 nm) are extremely small. It is, therefore, expected that the crystallized glasses having large Ω_2 parameters would show strong yellow emissions ($^4F_{9/2} \rightarrow {}^6H_{13/2}$). Indeed, as can be seen in Figs. 5, 7, and 8, the Ω_2 parameter in the crystallized glasses of $40BaO–20TiO_2–40SiO_2–0.5Dy_2O_3$ increases with increasing heat treatment temperature and the intensity of yellow emissions also increases. Since the change in the Ω_6 parameter due to the crystallization is small (Fig. 8), the intensity of blue emissions ($^4F_{9/2} \rightarrow {}^6H_{15/2}$) would not be expected to change largely. From these points, it is considered that the yellow/blue intensity ratio increases due to the crystallization, as seen in Fig. 7. It should be pointed out that the optical absorption edge in the crystallized glasses shifts to longer wavelengths (Fig. 2) and these shifts might give decreases in the intensity of blue emissions due to re-absorptions. From the above discussion, it is suggested that the site environment of Dy^{3+} ions changes largely due to the crystallization, and the large increase in the Ω_2 parameter indicates that the site symmetry of Dy^{3+} ions in crystallized glasses is largely asymmetric compared with that in the precursor glass.

The average bond character in isotropic materials such as glasses and nanocrystals, i.e., the degree of covelency or ionicity, has been discussed from the point of the electronic polarizability of oxygen ions [30–33]. By using the well-known Lorentz–Lorenz equation and the relationship between molar polarizability and electronic polarizability of oxide ions (α_{O2-}) [17,30–33], the values of $\alpha_{O_{2-}}$ for the crystallized glasses were evaluated, and the results are shown in Fig. 9. It is seen that the average electronic polarizability of oxygen ions decreases gradually with increasing heat treatment temperature. As proposed by Maruyama et al. [17], the decrease due to the crystallization would indicate the difference in the chemical bonding state of ions between BTS glass and $Ba_2TiSi_2O_8$ nanocrystal. That is, the data shown in Fig. 9 suggest that the chemical bonding state of constituent ions (Ba^{2+}, Ti^{4+}, Si^{4+}, Dy^{3+}) changes more to the covalent state due to the nanocrystallization of $Ba_2TiSi_2O_8$. The increase in the covalency of Dy^{3+}–O^2 bonds due to the crystallization also might contribute to the increase in the Ω_2 parameter shown in Fig. 8.

It is known that the PL quantum yield of RE ions in glasses depends on the maximum phonon energy, $\hbar\omega_{max}$, of a given matrix. In glasses (e.g., SiO_2-based glasses) having high maximum phonon energies, the emission intensity tends to decrease due to the multi-phonon relaxation process. Contrary, in glasses (e.g., TeO_2-based glasses) having low maximum phonon energies, the probability of multi-phonon relaxations decreases, consequently the emission intensity tends to increase. It is, therefore, of importance to estimate maximum phonon energies of the precursor BTS glass and crystallized glasses. For this purpose, we prepared $40BaO–20TiO_2–40SiO_2–0.5Eu_2O_3$ glass, and the phonon energies coupled with Eu^{3+} ions were estimated from the phonon

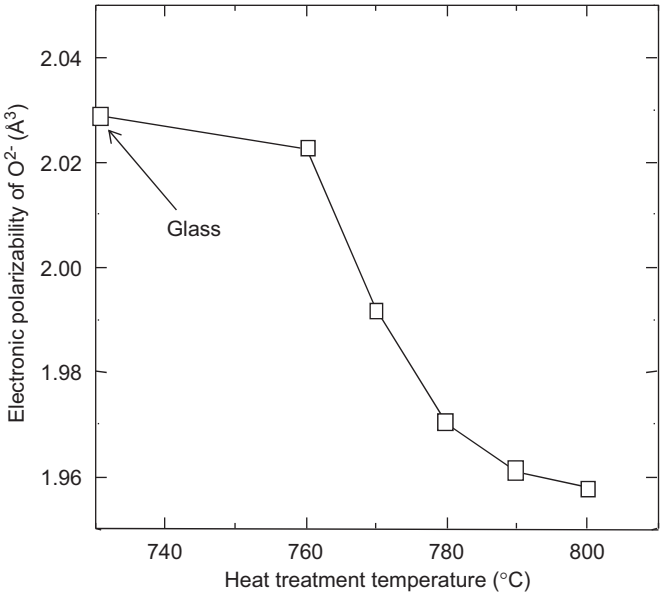

Fig. 9. Values of electronic polarizability of oxygen ions as a function of heat treatment temperature in the precursor BTS and crystallized glasses.

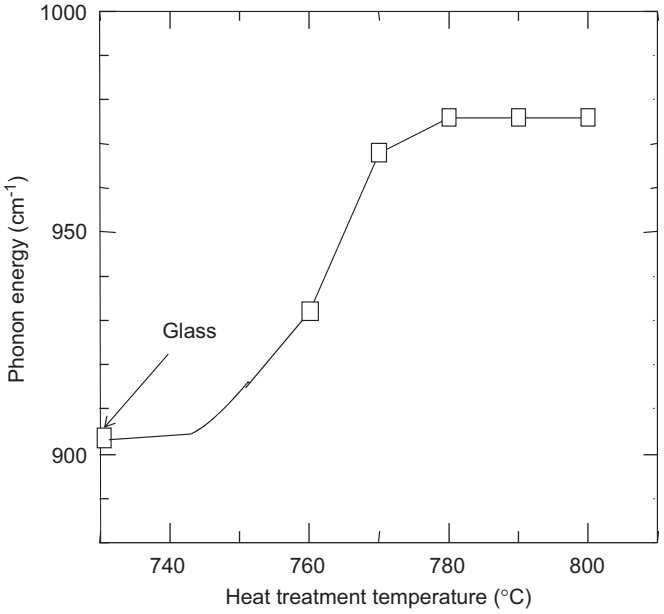

Fig. 10. Phonon energies coupled with Eu^{3+} ions of the precursor BTS and crystallized glasses, which were estimated from the phonon side bands of Eu^{3+} ions in $40BaO–20TiO_2–40SiO_2–0.5Eu_2O_3$ glass.

side bands of Eu^{3+} ions [16,34,35]. The results are shown in Fig. 10. The precursor glass has the value of 904 cm^{-1}, and the crystallized (780–800 °C) glasses show the values of 976 cm^{-1}. Although the change in the phonon energy is not large (72 cm^{-1}), the results shown in Fig. 10 suggest that the phonon energy coupled with RE^{3+} ions tends to increase due to the crystallization. From the point of the multi-phonon relaxations, it is expected that the emission intensity would decrease due to the crystallization. However, as clarified in this study, the emission intensity of Dy^{3+} ions in the visible region increases. It is, therefore, suggested that the PL intensity of Dy^{3+} ions in the crystallized glasses of $40BaO–20TiO_2–40SiO_2–0.5Dy_2O_3$ depends strongly on the state of the site symmetry and at least the contribution of the multi-

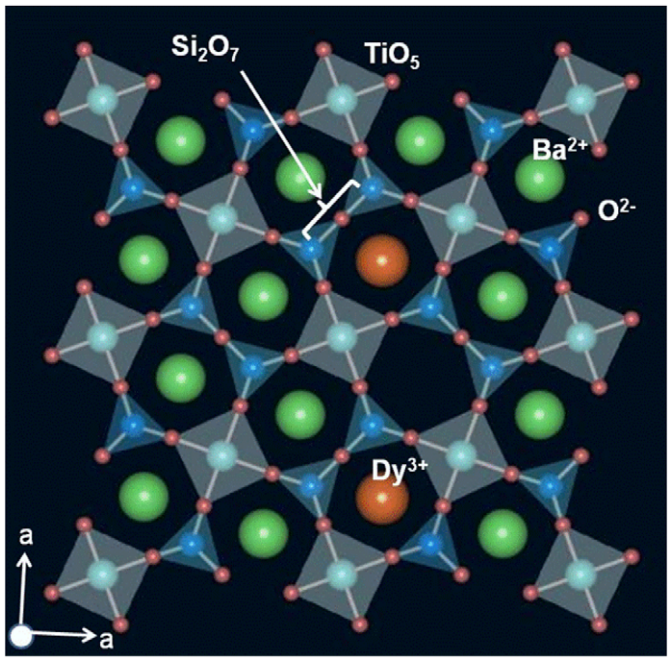

Fig. 11. Structural model for Dy^{3+} ions incorporated into nonlinear optical $Ba_2TiSi_2O_8$ nanocrystals in crystallized glasses. The project plane is the *c*-plane.

phonon relaxation would be small compared with the state of the site symmetry.

From the experimental results, it is concluded that Dy^{3+} ions are incorporated into $Ba_2TiSi_2O_8$ nanocrystals formed during the crystallization, as similar to Nd^{3+} and Er^{3+} ions [17]. Considering the ionic radius ($r = 0.1027$ nm) of Dy^{3+} ions, the most probable incorporation site in $Ba_2TiSi_2O_8$ crystals for Dy^{3+} ions would be the site of Ba^{2+} with the ionic radius of $r = 0.142$ nm. Furthermore, in order to maintain electrical neutrality in Dy^{3+}-doped $Ba_2TiSi_2O_8$ crystals, some amounts of vacancy might be formed in Ba^{2+} sites. The schematic structure model based on this discussion is shown in Fig. 11. It is also pointed out that $Ba_2TiSi_2O_8$ crystal itself has an anisotropic structure, inducing strong SHGs. Consequently, the site symmetry of Dy^{3+} ions incorporated into $Ba_2TiSi_2O_8$ nanocrystals would be largely anisotropic. On the other hand, the site symmetry of Dy^{3+} ions in the precursor BTS glass would be more symmetric as average because of the randomness and flexibility in the glass structure. It should be also pointed out that the size of $Ba_2TiSi_2O_8$ crystals formed during the crystallization of $40BaO–20TiO_2–40SiO_2–0.5Dy_2O_3$ glass is a nanoscale. This feature might be an origin for the broad PL emission peaks (with no fine structures) shown in Fig. 5.

The volume fraction of $Ba_2TiSi_2O_8$ nanocrystals in the crystallized glasses of $40BaO–20TiO_2–40SiO_2–0.5Dy_2O_3$ increases with increasing heat treatment temperature, e.g., $f = 0.64$ and 0.71 for the samples heat-treated at 780 and 800 °C for 30 min, respectively. It is, therefore, considered that Dy^{3+} ions would be present in the glassy phase, in the grain boundaries between the glassy phase and crystalline phase, and in the $Ba_2TiSi_2O_8$ nanocrystalline phase, although their fractions are unclear at this moment. It should be, however, again pointed out that the composition of the precursor BTS glass is the same as that of $Ba_2TiSi_2O_8$ nanocrystals. Consequently, the data obtained in the present study strongly suggest that the fraction of Dy^{3+} ions incorporated into $Ba_2TiSi_2O_8$ nanocrystals increases with increase in the volume fraction of $Ba_2TiSi_2O_8$ nanocrystals formed during the crystallization. That is, the optical properties of Dy^{3+} ions obtained in the crystallized glasses indicate largely the optical properties of Dy^{3+}-doped $Ba_2TiSi_2O_8$ nanocrystals.

4. Conclusions

The transparent crystallized glasses consisting of nonlinear optical $Ba_2TiSi_2O_8$ nanocrystals (diameter: ~100 nm) were prepared through the crystallization of $40BaO–20TiO_2–40SiO_2–0.5 Dy_2O_3$ glass, and the PL quantum yields of Dy^{3+} ions in the visible region were evaluated directly by using a PL spectrometer with an integrating sphere. The incorporation of Dy^{3+} ions into $Ba_2TiSi_2O_8$ nanocrystals was confirmed from the X-ray diffraction analyses. The total quantum yields of the emissions at the bands of $^4F_{9/2}\rightarrow{}^6H_{15/2}$ (484 nm), $^4F_{9/2}\rightarrow{}^6H_{13/2}$ (575 nm), and $^4F_{9/2}\rightarrow{}^6H_{11/2}$ (669 nm) in the crystallized glasses were ~15%, being about four times larger compared with the precursor glass. It was found that the intensity of yellow (575 nm) emissions and the branching ratio of the yellow (575 nm)/blue (484 nm) intensity ratio increase largely due to the crystallization. It was suggested from Judd–Ofelt analyses that the site symmetry of Dy^{3+} ions in the crystallized glasses is largely distorted, giving a large increase in the yellow emissions.

Acknowledgment

This work was supported by a Grant-in-Aid for Scientific Research from the Ministry of Education, Science, Sports, Culture and Technology, Japan.

References

[1] S. Tanabe, J. Kang, T. Hanada, N. Soga, J. Non-cryst. Solids 239 (1998) 170.
[2] P. Babu, C.K. Jayasankar, Opt. Mater. 15 (2000) 65.
[3] A. Thulasiramudu, S. Buddhudu, Spectrochim. Acta A 67 (2007) 802.
[4] R. Praveena, R. Vijaya, C.K. Jayasankar, Spectrochim. Acta A 70 (2008) 577.
[5] A. Herrmann, D. Ehrt, J. Non-cryst. Solids 354 (2008) 916.
[6] G.H. Beall, L.R. Pinckney, J. Am. Ceram. Soc. 82 (1999) 5.
[7] R. Sakai, Y. Benino, T. Komatsu, Appl. Phys. Lett. 77 (2000) 2188.
[8] F. Torres, K. Narita, Y. Benino, T. Fujiwara, T. Komatsu, J. Appl. Phys. 94 (2003) 5265.
[9] N.S. Prasad, K.B.R. Varma, Y. Takahashi, Y. Benino, T. Fujiwara, T. Komatsu, J. Solid State Chem. 173 (2003) 209.
[10] Y. Takahashi, K. Kitamura, Y. Benino, T. Fujiwara, T. Komatsu, Appl. Phys. Lett. 86 (2005) 091110.
[11] N. Iwafuchi, S. Mizuno, Y. Benino, T. Fujiwara, T. Komatsu, M. Koide, K. Matusita, Adv. Mater. Res. 11/12 (2006) 209.
[12] S. Mizuno, Y. Benino, T. Fujiwara, T. Komatsu, Jpn. J. Appl. Phys. 45 (2006) 6121.
[13] J. Capmany, D. Jaque, J.G. Sole, A.A. Kaminskii, Appl. Phys. Lett. 72 (1998) 531.
[14] G. Aka, A. Brenier, Opt. Mater. 22 (2003) 89.
[15] K. Hirano, Y. Benino, T. Komatsu, J. Phys. Chem. Solid 62 (2001) 2075.
[16] K. Naito, Y. Benino, T. Fujiwara, T. Komatsu, Solid State Commun. 131 (2004) 289.
[17] N. Maruyama, T. Honma, T. Komatsu, J. Chem. Phys. 128 (2008) 184706.
[18] M.J. Dejneka, J. Non-cryst. Solids 239 (1998) 149.
[19] M. Kusatsugu, M. Kanno, T. Honma, T. Komatsu, J. Solid State Chem. 181 (2008) 1176.
[20] A.A. Cabral, V.M. Fokin, E.D. Zanotto, C.R. Chinaglia, J. Non-cryst. Solids 330 (2003) 174.
[21] Y. Takahashi, K. Kitamura, S. Inoue, Y. Benino, T. Fujiwara, T. Komatsu, J. Ceram. Soc. Jpn. 113 (2005) 419.
[22] I. Enomoto, Y. Benino, T. Fujiwara, T. Komatsu, J. Ceram. Soc. Jpn. 114 (2007) 374.
[23] R.D. Shannon, Acta Cryst. A 32 (1976) 751.
[24] S. Haussühl, J. Eckstein, K. Recker, F. Wallrafen, J. Cryst. Growth 40 (1977) 200.
[25] C.K. Jørgensen, R. Reisfeld, J. Less-common Met. 93 (1983) 107.
[26] E.W.J.L. Oomen, A.M.A. van Dongen, J. Non-cryst. Solids 111 (1989) 205.
[27] Y. Nageno, H. Takebe, K. Morinaga, J. Am. Ceram. Soc. 76 (1993) 3081.
[28] S. Tanabe, T. Hanada, T. Ohyagi, N. Soga, Phys. Rev. B 48 (1993) 10591.
[29] S. Tanabe, T. Ohyagi, N. Soga, T. Hanada, Phys. Rev. B 46 (1992) 3305.
[30] V. Dimitrov, S. Sakka, J. Appl. Phys. 79 (1996) 1736.
[31] J.A. Duffy, M.D. Ingram, J. Am. Chem. Soc. 93 (1971) 6448.
[32] V. Dimitrov, T. Komatsu, J. Solid State Chem. 163 (2002) 100.
[33] V. Dimitrov, T. Komatsu, J. Solid State Chem. 178 (2005) 831.
[34] S. Tanabe, S. Yoshii, K. Hirao, N. Soga, Phys. Rev. B 45 (1992) 4620.
[35] H. Oishi, Y. Benino, T. Komatsu, Phys. Chem. Glasses 40 (1999) 212.